Biochimica et Biophysica Acta 1833 (2013) 2254–2266

Contents lists available at SciVerse ScienceDirect

Biochimica et Biophysica Acta

journal homepage: www.elsevier.com/locate/bbamcr

N-terminally truncated forms of human cathepsin F accumulate in aggresome-like inclusions☆,☆☆

Barbara Jerič [a,b], Iztok Dolenc [a], Marko Mihelič [a,c], Martina Klarić [a,b], Tina Zavašnik-Bergant [a], Gregor Gunčar [d], Boris Turk [a,b,c,d], Vito Turk [a,b,c,*], Veronika Stoka [a,b,**]

[a] Department of Biochemistry and Molecular and Structural Biology, J. Stefan Institute, Jamova 39, SI-1000 Ljubljana, Slovenia
[b] Jožef Stefan International Postgraduate School, Jamova 39, SI-1000 Ljubljana, Slovenia
[c] Centre of Excellence for Integrated Approaches in Chemistry and Biology of Proteins (CIPKeBiP), Jamova 39, SI-1000 Ljubljana, Slovenia
[d] Department of Chemistry and Biochemistry, Faculty of Chemistry and Chemical Technology, University of Ljubljana, Cesta v Mestni log 88A, SI-1000 Ljubljana, Slovenia

ARTICLE INFO

Article history:
Received 19 November 2012
Received in revised form 6 May 2013
Accepted 7 May 2013
Available online 14 May 2013

Keywords:
Aggregation-prone
Aggresome
Aggresome-like inclusion
Autophagy
Caspase activation
Cathepsin F

ABSTRACT

The contribution of individual cysteine cathepsins as positive mediators of programmed cell death is dependent on several factors, such as the type of stimuli, intensity and duration of the stimulus, and cell type involved. Of the eleven human cysteine cathepsins, cathepsin F is the only cathepsin that exhibits an extended N-terminal proregion, which contains a cystatin-like domain. We predicted that the wild-type human cathepsin F contains three natively disordered regions within the enzyme's propeptide and various amino acid stretches with high fibrillation propensity. Wild-type human cathepsin F and its N-terminally truncated forms, Ala^{20}–Asp^{484} (Δ^{19}CatF), Pro^{126}–Asp^{484} (Δ^{125}CatF), and Met^{147}–Asp^{484} (Δ^{146}CatF) were cloned into the pcDNA3 vector and overexpressed in HEK 293T cells. Wild-type human cathepsin F displayed a clear vesicular labeling and colocalized with the LAMP2 protein, a lysosomal marker. However, all three N-terminally truncated forms of human cathepsin F were recovered as insoluble proteins, suggesting that the deletion of at least the signal peptides (Δ^{19}CatF), results in protein aggregation. Noteworthy, they concentrated large perinuclear–juxtanuclear aggregates that accumulated within aggresome-like inclusions. These inclusions showed p62-positive immunoreactivity and were colocalized with the autophagy marker LC3B, but not with the LAMP2 protein. In addition, an approximately 2–3 fold increase in DEVDase activity was not sufficient to induce apoptotic cell death. These results suggested the clearance of the N-terminally truncated forms of human cathepsin F via the autophagy pathway, underlying its protective and prosurvival mechanisms.

1. Introduction

During the past decade, there has been an expansion of studies highlighting the importance of cysteine cathepsins under various physiological and pathological conditions [1]. Novel functions have been uncovered, and their involvement in the activation of programmed cell death (apoptosis) has been confirmed [2–7]. The contribution of cysteine cathepsins to apoptosis varies considerably and is dependent on the initiation of stimuli targeting in the mitochondria (*intrinsic* pathway) or activation of death receptors (*extrinsic* pathway) [8–13]. Studies aimed at dissecting the contribution of individual enzymes as positive mediators of apoptosis have also provided conflicting results. The transient overexpression of aspartic cathepsin D demonstrated several features of apoptosis, as assessed by cell morphology, DNA fragmentation and/or caspase-3 enzymatic activity [14]. In contrast, the transient overexpression of cysteine cathepsin B or cathepsin L did not demonstrate any significant features of apoptosis in either HeLa or rat hepatoma McA RH 7777 cell lines [15]. A 20-fold overexpression of these cysteine cathepsins or lysosomal permeabilization with the lysosomotropic detergent, *N*-dodecyl-imidazole, was insufficient to sensitize these cells to TNF-induced cell death [15]. In contrast, cathepsin B alternatively spliced variants and artificially truncated forms were found in various cellular compartments and induced apoptotic cell death [16–18]. Moreover, cysteine cathepsins B, H and L and the aspartic cathepsin D were detected in tubulovesicular structures surrounding the chromatoid bodies, which

Abbreviations: Δ^{19}CatF, truncated form of human cathepsin F (Ala^{20}–Asp^{484}); Δ^{125}CatF, truncated form of human cathepsin F (Pro^{126}–Asp^{484}); Δ^{146}CatF, truncated form of human cathepsin F (Met^{147}–Asp^{484}); HRP, horseradish peroxidase; Mw, molecular weight; wtCatF, wild-type cathepsin F

☆☆ This paper is dedicated to Prof. John A. Rupley at the Department of Chemistry and Biochemistry, University of Arizona, Tucson on the occasion of his 80th birthday.

* Correspondence to: V. Turk, J. Stefan Institute, Department of Biochemistry and Molecular and Structural Biology, Jamova 39, SI-1000 Ljubljana, Slovenia. Tel.: +386 1 477 3365; fax: +386 1 477 3984.

** Correspondence to: V. Stoka, J. Stefan Institute, Department of Biochemistry and Molecular and Structural Biology, Jamova 39, SI-1000 Ljubljana, Slovenia. Tel.: +386 1 477 3854; fax: +386 1 477 3984.

E-mail addresses: vito.turk@ijs.si (V. Turk), veronika.stoka@ijs.si (V. Stoka).

0167-4889/$ – see front matter © 2013 The Authors. Published by Elsevier B.V. All rights reserved.
http://dx.doi.org/10.1016/j.bbamcr.2013.05.007

displayed aggresome-like characteristics, and were confirmed to be a degradation site for unnecessary DNA, RNA, and proteins rather than a synthesis site [19]. Since cathepsin F (CTSF) has an unusually long N-terminal proregion [20,21] and is the only cysteine cathepsin whose inactivation alone results in a lysosomal storage defect and progressive neurological features in mice [22], we sought to determine whether this enzyme may also play a role in cell death.

In this study, wtCatF and its N-terminally truncated forms Ala^{20}–Asp^{484} (Δ^{19}CatF), Pro^{126}–Asp^{484} (Δ^{125}CatF) and Met^{147}–Asp^{484} (Δ^{146}CatF) were overexpressed in HEK 293T cells. We confirmed the protein's expression level, distinct subcellular localization and involvement in caspase activation and aggresome formation. In addition, a bioinformatic analysis highlighted the presence of natively disordered regions within the human cathepsin F sequence and its fibrillation propensity. Moreover, we demonstrated that all three N-terminally truncated forms of human cathepsin F accumulated in aggresome-like inclusions, and were confirmed as p62-positive aggregates, which differed from the wild-type protein.

2. Materials and methods

2.1. Reagents

All of the reagents were of an analytical grade and were purchased from Sigma-Aldrich (St. Louis, MO, USA) unless otherwise stated. The human embryonic kidney 293T (HEK 293T) cell line was purchased from LGC Standards GmbH (Wesel, Germany). Phosphate-buffered saline (PBS), Dulbecco's modified Eagle's medium (DMEM), fetal bovine serum, L-glutamine and penicillin/streptomycin were obtained from PAA (Piscataway, NJ, USA). Poly-L-lysine, the protein inhibitor cocktail and the mouse monoclonal anti-β-actin antibody clone AC-15 (#A1978) were obtained from Sigma-Aldrich (St. Louis, MO, USA). The Xfect transfection reagent was purchased from Clontech (Mountain View, CA, USA). The pcDNA3 vector, non-animal cell dissociation reagent TrypLE Select, ProLong Gold antifade reagent, SlowFade Gold antifade reagent with DAPI, goat anti-rabbit Alexa Fluor 488-conjugated secondary antibody, goat anti-mouse Alexa Fluor 546-conjugated secondary antibody and donkey anti-goat Alexa Fluor 546-conjugated secondary antibody were purchased from Life Technologies (Grand Island, NY, USA). The restriction enzymes HindIII and EcoRI and peptide: N-glycosidase (PNGase F) were obtained from New England Biolabs (Ipswich, MA, USA). The 15-mm round glass coverslips were obtained from Electron Microscopy Sciences (Hatfield, PA, USA). The Bio-Rad Protein assay was purchased from Bio-Rad (Hercules, CA, USA). The caspase substrate Ac-Asp-Glu-Val-Asp-AFC and pan-caspase inhibitor Z-Val-Ala-DL-Asp(OMe)-fluoromethylketone were purchased from Bachem AG (Bubendorf, Switzerland). Stock solutions of substrate and inhibitor were prepared in dimethylsulfoxide and stored at −20 °C until further use. ProteoStat® Aggresome Detection kit was obtained from Enzo Life Sciences (Plymouth Meeting, PA, USA). Rabbit anti-human cathepsin F polyclonal antibody (#sc-13987) was purchased from Santa Cruz Biotechnology (Santa Cruz, CA, USA) whereas the goat anti-human cathepsin F polyclonal antibody (#ab36161), mouse monoclonal anti-human LAMP2 antibody [H4B4] (#ab25631), rabbit polyclonal anti-human LC3B antibody (#ab51520) and donkey anti-goat HRP-conjugated secondary polyclonal antibody (#ab6885) were obtained from Abcam (Cambridge, MA, USA). Mouse monoclonal anti-human p62/SQSTM1, clone 11C9.2 antibody (#MABC32) was obtained from Merck Millipore (Darmstadt, Germany). Goat anti-mouse HRP-conjugated secondary polyclonal antibody (#115-035-068) was obtained from Jackson ImmunoResearch Laboratories (West Grove, PA, USA).

2.2. Plasmid construction

The pPCR-Script plasmid containing the wild-type human cathepsin F (IMAGE clone 3637189 (Invitrogen, Carlsbad, USA) was used as a template. The cloning was performed using the following oligonucleotide sequences for wild-type human cathepsin F (forward primer: 5′-ggaaagcttaaaatggcgccctggctg-3′, reverse primer: 5′-atgaattctcagtc caccaccgccg-3′) whereas for the N-terminally truncated forms Ala^{20}–Asp^{484} (Δ^{19}CatF) (forward primer: 5′-ggaaagcttatggcccccgcccagc-3′, reverse primer: 5′-atgaattctcagtccaccaccgcc-3′), Pro^{126}–Asp^{484} (Δ^{125}CatF) (forward primer: 5′-ggaaagcttatgccagtggacaccaag-3′, reverse primer: 5′-atgaattctcagtccaccaccgccg-3′), and Met^{147}–Asp^{484} (Δ^{146}CatF) (forward primer: 5′-ggaaagcttatgatttcttctctgtccc-3′, reverse primer: 5′-atgaattctcagtccaccaccgcc-3′). Wild-type human cathepsin F and the chimeric constructs were inserted into the mammalian expression vector pcDNA3 using HindIII and EcoRI restriction enzymes.

2.3. Cell culture and transfection

HEK 293T cells were grown in DMEM medium supplemented with 10% (v/v) fetal bovine serum, 2 mM L-glutamine, 100 U/ml penicillin and 100 μg/ml streptomycin at 37 °C in a humidified atmosphere with 5% CO_2. Cells were evenly seeded and grown overnight before treatment. For the immunofluorescence labeling and aggresome detection studies, HEK 293T cells were grown on poly-L-lysine-coated coverslips.

The plasmids were transfected into the cells using the Xfect transfection reagent according to the manufacturer's instructions and grown in complete growth media alone or supplemented with 15 μM Z-VAD(OMe)-FMK for 48 h prior to the analysis. Negative controls included non-transfected, mock and empty vector-transfected cells.

2.4. Preparation of whole cell extracts

The cells were harvested 48 h after transfection using TrypLE Select, washed twice with PBS and centrifuged for 5 min at 1000 ×*g*. The supernatant was discarded, and the pellet was resuspended in ice-cold RIPA buffer (50 mM Tris, 100 mM NaCl, 0.1% (w/v) SDS, 1% (v/v) NP-40, 0.5% (w/v) deoxycholic acid, 1 mM EDTA pH 8.0). A cocktail of inhibitors was added to the RIPA buffer to prevent protein degradation prior to Western blotting. The cells were disrupted by 1 h incubation period on ice and spun for 10 min at 16,000 ×*g* using a refrigerated microcentrifuge (Eppendorf 5415R). The supernatant (soluble fraction) was collected and either used immediately or stored at −20 °C for later use. The pellet (insoluble fraction) was further processed with slight modifications from Johnston et al. [23]. Briefly, the pellets were solubilized in 50 μl of 1% (v/v) SDS in PBS for 10 min at room temperature, followed by addition of 50 μl RIPA buffer and sonicated for 10 s using a tip sonicator Branson W-450D (Branson, Danbury, CT, USA).

2.5. Determination of protein concentration

The protein concentration was estimated using the Bio-Rad Protein assay, on the basis of the Bradford method, according to the manufacturer's instructions (Bio-Rad).

2.6. Cathepsin F deglycosylation

N-linked glycosylation of wtCatF was assessed upon treatment with peptide: N-glycosidase (PNGase F) according to the manufacturer's instructions (New England Biolabs). The glycoprotein denaturing buffer (final conc. 0.5% SDS, 40 mM DTT) was added to 20 μg total protein obtained from whole cell extracts and the mixture was heated at 100 °C for 10 min. Next, PNGase F (1500 U final) resuspended in 50 mM sodium phosphate buffer pH 7.5 containing 1% NP40 was added to the above mixture to a final reaction volume of 20 μl and incubated at 37 °C for 1 h. An analogous reaction was performed in the absence of PNGase F, which was used as a negative control. A decrease in

the molecular weight of the protein band upon deglycosylation was assessed using Western blotting as described in Section 2.8.

2.7. Caspase activity detection

Caspase (DEVDase) activities were assessed from 50 μg of total protein. Briefly, the cleavage of the fluorogenic substrate Ac-DEVD-AFC was continuously measured in a 96-well plate reader (Tecan Infinite M1000 PRO, Männedorf, Switzerland) at excitation and emission wavelengths of 400 nm and 505 nm, respectively. The steady-state rates of substrate hydrolysis were extrapolated from the linear phase of the progression curves.

2.8. SDS-PAGE and Western blotting

A total of 20 μg of protein extract was loaded and resolved in 12.5% SDS-PAGE gels, which were run under reducing conditions using 25 mM Tris, 0.2 M glycine, 0.1% (w/v) SDS running buffer (35 mA constant per gel). The gels were then electro-transferred on to nitrocellulose membrane (Serva Electrophoresis GmbH, Heidelberg, Germany) at 250 mA constant over 120 min in buffer containing 25 mM Tris, 8 mM glycine and 20% (v/v) methanol. After the blocking step, the membranes were probed using goat polyclonal anti-human cathepsin F antibody (final conc. 0.5 μg/ml) for 3 h. The membranes were washed and then incubated with donkey anti-goat HRP-conjugated polyclonal secondary antibody (final conc. 0.17 μg/ml) for 1 h at room temperature. Next, the antigen/antibody complexes were detected using ECL Plus Western blotting detection reagents according to the manufacturer's instructions (GE Healthcare Bio-Sciences AB, Uppsala, Sweden). The membrane was exposed to Kodak BioMax Light autoradiography film and developed using a Konica Minolta SRX-101A automatic X-ray film processor (Konica Minolta, Tokyo, Japan). Protein loading was assessed by reprobing the Western blots using mouse monoclonal antibody against β-actin (final conc. 0.5 μg/ml) and the goat anti-mouse HRP-conjugated polyclonal secondary antibody (final conc. 0.13 μg/ml).

2.9. Immunolabeling and confocal microscopy

HEK 293T cells were grown on poly-L-lysine-coated coverslips and transfected as previously described in Section 2.3. Prior to immunofluorescence labeling, the cells were fixed and permeabilized in ice-cold methanol for 13 min on ice, rinsed in PBS and further incubated in blocking buffer (3% BSA in PBS) for 30 min. Cells were then incubated with a polyclonal rabbit anti-human cathepsin F antibody, goat polyclonal anti-human cathepsin F antibody, mouse monoclonal anti-LAMP2 antibody [H4B4], rabbit polyclonal anti-human LC3B antibody or mouse monoclonal anti-human p62/SQSTM1 antibody at a final concentration of 1 μg/ml for 45 min for a single or double immunolabeling and washed with PBS. The cells were further incubated with the appropriate secondary antibody (goat anti-rabbit, goat anti-mouse or donkey anti-goat) conjugated either with Alexa Fluor 488 or Alexa Fluor 546 at a final concentration of 0.8 μg/ml for 45 min and washed several times with PBS. Labeled cells were mounted using the SlowFade Gold antifade reagent with DAPI (blue-fluorescent nuclear stain), which eliminated the need for a separate counterstaining step. The controls were processed in the absence of the primary antibody.

Fluorescence microscopy and optical slicing were performed using an inverted confocal laser scanning microscope LEICA TCS SP5 X with white light laser (WLL) at an excitation source in the range from 470 nm to 670 nm and a 405 nm diode laser for DAPI excitation. The excitation lines were selected using an acousto-optical tunable filter (AOTF) as indicated below. An oil objective HCX PL APO 60× (N.A. = 1.4) was used. Optical sections in the z-direction were obtained and the emission signal was separated using an acousto-optical beam splitter (AOBS) and captured with one PMT and two hybrid detectors (HyD). Immunolabeled cathepsin F, LAMP2, p62/SQSTM1 and LC3B were excited using the 488 nm and 546 nm lines from WLL. Sequential scanning was strictly applied when multiple fluorescence signals were examined and the emission light was detected within the range of (1) 413 nm–457 nm for fluorescence in the blue spectrum, (2) 498 nm–550 nm for fluorescence in the green spectrum, and (3) 559 nm–617 nm for fluorescence in the red spectrum. Leica software LAS AF was used to evaluate the obtained fluorescence signals and colocalization of labeled proteins, respectively.

2.10. Aggresome detection

Cellular aggresomes were detected using the ProteoStat® Aggresome Detection kit according to the manufacturer's instructions (Enzo Life Sciences). HEK 293T cells were grown on poly-L-lysine coated coverslips and transfected as previously described in Section 2.3. The cells incubated for 12 h with a cell permeable proteasome inhibitor MG-132 (5 μM), which was used as a positive control. Next, the cells were washed with PBS and fixed in 4% paraformaldehyde for 30 min at room temperature. The cells were then permeabilized in permeabilizing solution (0.5% Triton X-100, 3 mM EDTA, pH 8.0 in 1× assay buffer) with gentle shaking on ice for 30 min. After this step, the cells were washed again in PBS and stained using the ProteoStat® Aggresome Detection Reagent and Hoechst 33342 nuclear stain for 30 min at room temperature protected from light. The microscope slides were mounted using the ProLong Gold antifade reagent and the aggresomes were visualized using an Olympus IX81 microscope (Olympus, Tokyo, Japan) with a motorized fluorescence unit. The emission signal was filtered using U-N49002 (green fluorescence) and U-M41002 (red fluorescence) filter cubes. Oil immersion objective UPlanSApo 100× (N.A. = 1.35) was used. Micrographs were obtained using a Hamamatsu ORCA-R^2 CCD camera (Hamamatsu, Hamamatsu City, Japan), and the Olympus Cell F software (Olympus, Tokyo, Japan) was used to evaluate the fluorescence signals.

2.11. Bioinformatics analysis tools

2.11.1. Prediction of molecular weight

The theoretical average molecular weight for human cathepsin F and its truncated forms were calculated using the deposited protein sequence (UniProt ID: Q9UBX1), as previously described [24].

2.11.2. Prediction of protein disorder

The prediction of natively disordered regions within the human cathepsin F amino acid sequence was performed using a meta Protein Disorder Prediction System (metaPrDOS), which is a meta server that integrates the results of the following prediction algorithms: PrDOS, DISOPRED2, DisEMBL, DISOclust, DISpro, DISPROT (VSL2), IUpred and POODLE-S [25].

2.11.3. Prediction of aggregation-prone regions

The prediction of aggregation-prone regions in human cathepsin F was performed using the 3D profile method, which consisted of an ensemble of templates derived from the crystal structure of the peptide NNQQNY, a representative of cross-β spines [26,27]. Segments with binding energies below an empirical threshold value of −23 kcal/mol were predicted to form fibrils [26]. A high fibrillation propensity was referred to as a "steric-zipper" which are two self-complementary β-sheets that form the spine of an amyloid fibril [26,27].

2.11.4. 3D-protein modeling

Three dimensional atomic models of the truncated form of human cathepsin F (Pro^{126}–Asp^{484}) and procathepsin F (Ser^{176}–Asp^{484}) were generated using the iterative implementation of the Threading ASSEmbly Refinement (I-TASSER) program [28,29]. Briefly, the I-TASSER protocol consisted of the following steps: 1) threading, 2) structural assembly, 3)

model selection and refinement and 4) a structure-based functional annotation [29].

3. Results and discussion

3.1. Human cathepsin F contains three natively disordered regions and various amino acid stretches with high fibrillation propensity

The amino acid sequence might be a determinant of protein aggregation and/or amyloidogenicity [30,31]. Thus, we assessed the potential contribution of amino acid stretches indicative of natively disordered regions and/or a propensity for aggregation within the primary and tertiary structure of human cathepsin F. The prediction of intrinsically disordered regions was performed using the meta Protein Disorder Prediction System (metaPrDOS) server, which integrated the results of eight prediction algorithms [25]. The consensus approach suggested three natively disordered regions within the enzyme's propeptide (Fig. 1). Peak 1 was found within the cystatin-like domain and included the first 12 amino acid residues following the signal peptide (Arg^{20}–Arg^{31}). Peak 2 (Pro^{126}–Leu^{175}) and peak 3 (Arg^{245}–Leu^{270}) were found among the flexible linker regions. The latter connected the cystatin-like domain with the inhibitory_I29 domain and then with the peptidase C1A domain corresponding to the mature form of cathepsin F.

A detailed study involving a non-redundant set of ordered and disordered protein segments indicated significant differences between their amino acid compositions and sequence attribute values, i.e., coordination number, flexibility, aromaticity, net charge and hydropathy scales [32]. Moreover, a comparative study of the relationship between the protein structure and β-aggregation in globular and intrinsically disordered proteins (IDPs) demonstrated that globular proteins contained approximately three times as many aggregation nucleating regions, such as IDPs, whereas the formation of highly structured globular proteins occurred at the cost of a higher β-aggregation propensity due to their protein structure and aggregation properties, which obey very similar physico-chemical constraints [33].

Various sequence- and structure-based methods have been developed to predict the protein propensity for aggregation and/or amyloid-fibril formation [34,35]. A structure method based on the crystal structure of the cross-β spine steric zipper formed by the peptide NNQQNY enabled the identification of the fibril-forming segments of proteins that had been previously undetected [26]. A detailed structural study of 30 fibril-forming segments from 14 different proteins revealed eight classes of steric zippers where two identical β-sheets could be classified according to the orientation of their facing side chains (either 'face-to-face' or 'face-to-back'), the orientation of their strands (with both β-sheets having the same edge of the strand 'up', or one 'up' and the other 'down'), and whether the strands within the β-sheets were either parallel or antiparallel [36].

The amino acid sequence and location on the protein structure have been shown to be a determinant of aggregation and/or amyloid-fibril formation [37,38]. Thus, we generated a 3D model of Δ^{125}CatF. In addition, the location of the predicted natively disordered and aggregation-prone regions was labeled accordingly in the primary (Fig. 2A) and tertiary (Fig. 2B, C) structures of the protein.

Three-dimensional atomic models of Δ^{125}CatF were constructed from multiple threading alignments and iterative structural assembly simulations using I-TASSER, an integrated platform for protein structure prediction [28,29]. Although the protein topology of the best model was correctly assessed (TM score: 0.63 ± 0.14), the model's uncertainty predominantly relied on the first 60 amino acid residues due to the lack of sequence and structure conservation and the lack of appropriate templates (Fig. 2C). The latter was confirmed using a 3D model of procathepsin F (Ser^{176}–Asp^{484}), which was built in the absence of the 50-amino acid residue long linker region (Pro^{126}–Ile^{175}). The procathepsin F model provided a TM score value of 0.92 ± 0.06 and significantly improved the model's quality (46%).

The fibrillation propensity within human cathepsin F was assessed using a 3D profile [26] (Fig. 2A). This structure-based algorithm included contributions from apolar interactions, hydrogen bonds and steric overlaps, as well as retrieving amyloid-forming segments that might be undetected using property-based methods, i.e., hydrophobicity or β-strand propensity [26]. An energy per amino acid residue below −23 kcal/mol on the Rosetta Design energy scale was indicative of a high fibrillation propensity [26]. The findings obtained from the 3D profile were highlighted on the Δ^{125}CatF 3D model (Fig. 2B, C), where the aggregation-prone amino acid stretches were found to be solvent-exposed (Val^{181}–Ser^{185}, Gln^{143}–Ser^{150}) or mixed (Thr^{162}–Val^{166}). Additional aggregation-prone regions were predicted within the mature form of the enzyme (Fig. 2A), namely Gly^{281}–Ala^{282}, Ala^{341}–Ser^{343}, Ile^{400}–Ala^{403}, Ala^{432}–Val^{433} and Ala^{471}–Ala^{478}.

Although several factors have been shown to affect aggregation of proteins and peptides [32,39], various evolutionary strategies have been developed to prevent this from occurring (i) optimization of the thermodynamic stability of the protein is prevented burying the aggregation prone regions in solvent inaccessible regions of the structure, (ii) segregation between the folding nuclei and the aggregation nuclei

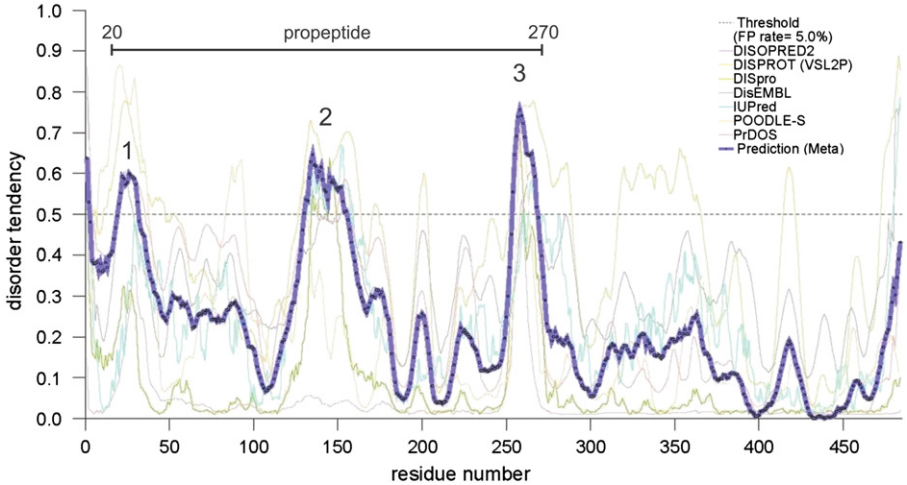

Fig. 1. Disorder profile of human cathepsin F. The probability of the disorder or disorder tendency within human cathepsin F was determined from its amino acid sequence using a consensus approach and a meta server (metaPrDOS) [25]. Three natively disordered regions (peaks 1–3) were found within the enzyme's propeptide region.

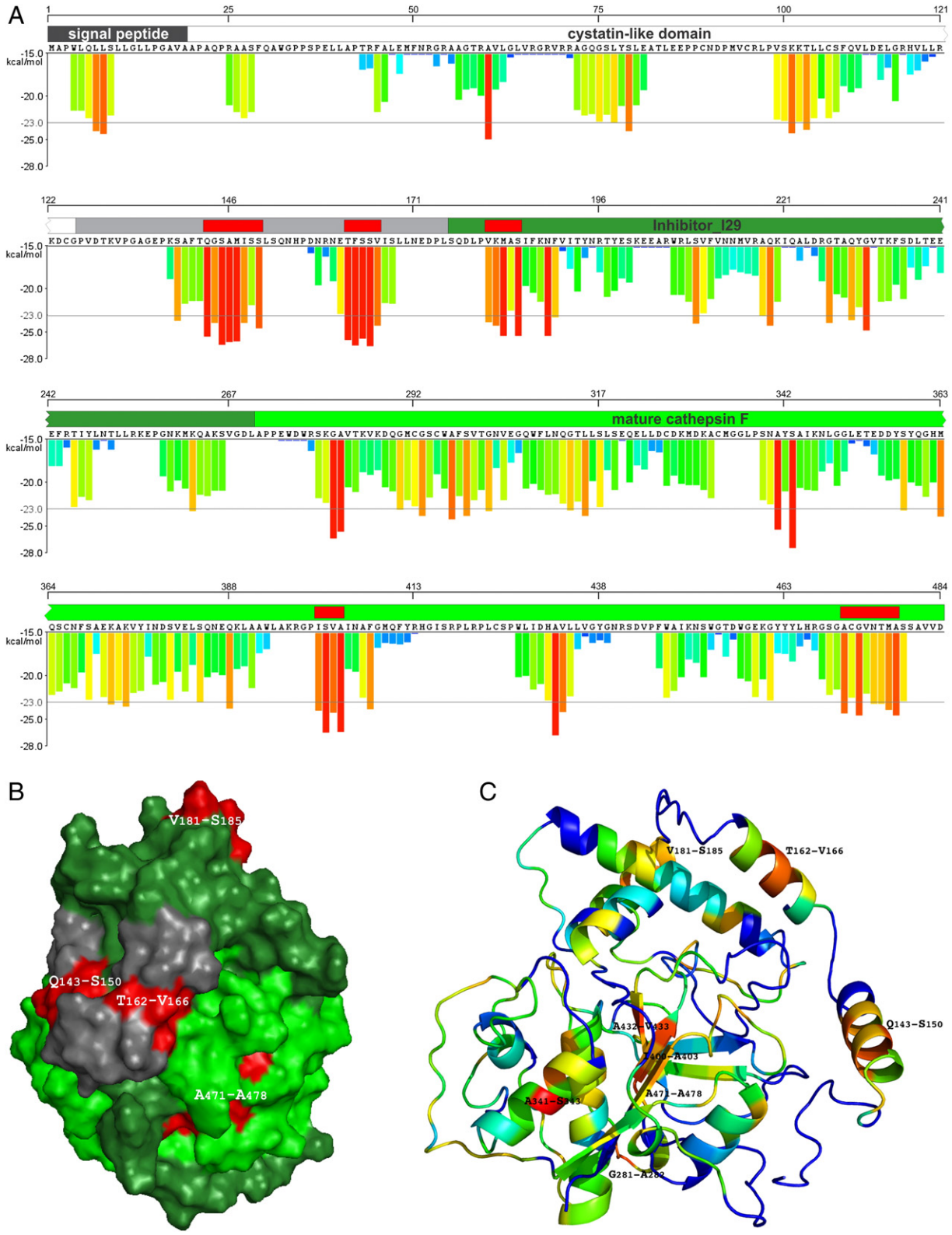

Fig. 2. Aggregation-prone regions of human cathepsin F. (A) The propensity for aggregation and/or amyloid fibril formation was determined using the 3D profile method [26]. The amino acid residues were colored according to their fibrillation propensity on a blue-to-red scale. The protein domain boundaries were indicated in the primary (A) and tertiary (B) structures of the protein. The non-conserved 50-amino acid residue region (P126–L175) is shown in dark gray, the inhibitor domain I29 (S176–L270) in dark green, and the mature form (A271–D484) in light green. Surface (B) and cartoon representation (C) of human Δ^{125}CatF. Δ^{125}CatF contains two exposed aggregation-prone amino acid stretches from positions Q143–S150 (energy range: −23.8 to −26.3 kcal/mol) and V181–S185 (energy range: −22.4 to −25.3 kcal/mol) and a mixed region at positions T162–V166 (energy range: −24.1 to −26.5 kcal/mol, mixed). Moreover, within the mature form of the enzyme, two major aggregation-prone regions were predicted from positions I400–A403 (energy range: −24.0 to −26.5 kcal/mol) and A471–A478 (energy range: −22.0 to −24.5 kcal/mol). These aggregation-prone amino acid stretches were highlighted in red in the primary (A) and tertiary (B) structures of the enzyme. The latter view (Fig. 2B) emphasizes their location at the enzyme's surface and is not the standard orientation used to display the structural data on the papain-like enzymes. The prediction of the 3D atomic model of Δ^{125}CatF was performed using the I-TASSER server [29]. A ribbon representation of the front view (standard orientation) of the best model is shown in panel C, which is labeled by their fibrillation propensity as assessed in panel A. The reliability of the model is indicated by a TM score: 0.63 ± 0.14. The molecular structure was generated using the molecular visualization system PyMOL [65].

Fig. 3. Schematic representation of human cathepsin F and its N-terminally truncated forms. The domain composition of wild-type human cathepsin F is indicated (top panel). The boundaries of the N-terminally truncated forms Ala^{20}–Asp^{484} (Δ^{19}CatF); Pro^{126}–Asp^{484} (Δ^{125}CatF) and Met^{147}–Asp^{484} (Δ^{146}CatF) are indicated accordingly in a scaled representation.

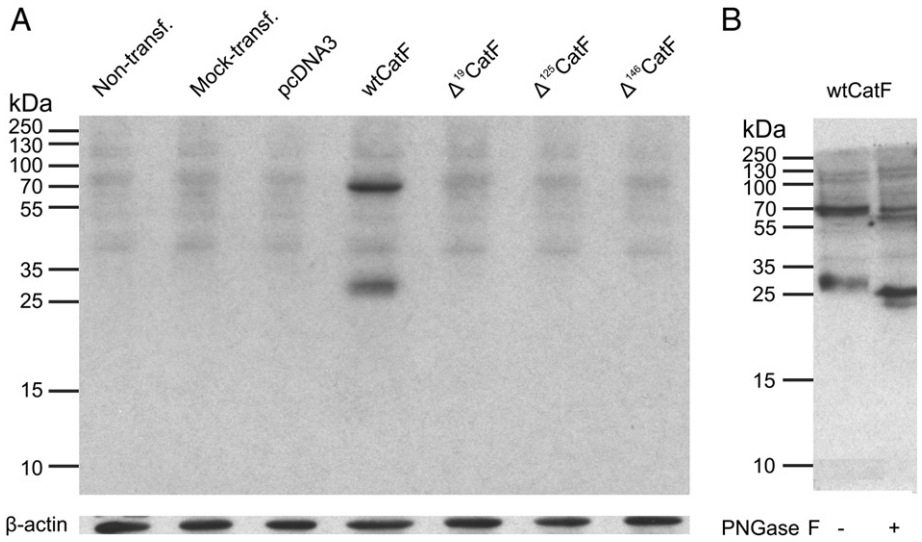

Fig. 4. (A) Expression of human cathepsin F and its N-terminally truncated forms in HEK 293T cells: soluble fraction. HEK 293T cells were transfected with pcDNA3-containing plasmids of human cathepsin F and its N-terminally truncated forms Δ^{19}CatF, Δ^{125}CatF and Δ^{146}CatF for 48 h. Next, whole cell protein extracts were evaluated by Western blotting analysis using an anti-human cathepsin F antibody (Abcam #ab36161). Negative controls included the non-transfected, mock-transfected and pcDNA3 empty vector-transfected cells. Loading of equivalent amounts of protein was assessed against β-actin (lower blot). (B) Deglycosylation of human cathepsin F by peptide: N-glycosidase (PNGase F). An extract of HEK 293T cells expressing wild-type human cathepsin F was treated with PNGase F and a decrease in Mw of the protein band upon N-deglycosylation was assessed by Western blotting.

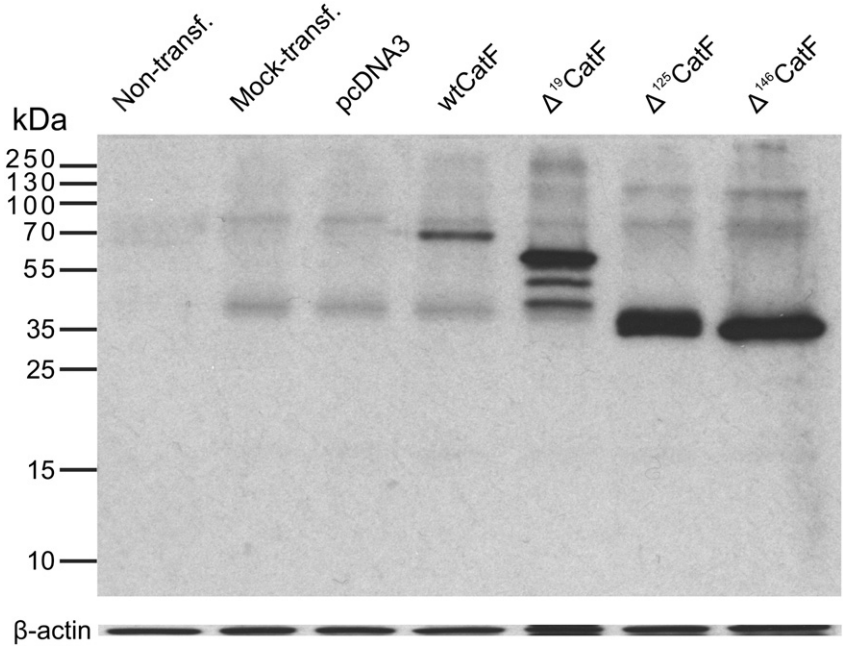

Fig. 5. Expression of human cathepsin F and its N-terminally truncated forms in HEK 293T cells: insoluble fraction. HEK 293T cells were transfected with pcDNA3-containing plasmids of human cathepsin F and its N-terminally truncated forms Δ^{19}CatF, Δ^{125}CatF and Δ^{146}CatF for 48 h. Next, whole cell protein extracts were evaluated by Western blotting analysis using an anti-human cathepsin F antibody (Abcam #ab36161). Negative controls included the non-transfected, mock-transfected and pcDNA3 empty vector-transfected cells. Loading of equivalent amounts of protein was assessed against β-actin (lower blot).

within a protein sequence, (iii) placement of gatekeeper residues at the flanks of aggregating segments, and (iv) molecular chaperones that directly target aggregation nucleating sequences in cellular environment [40]. Thus, the number of proteins that are capable of forming amyloid-like fibrils, which has been coined the "amylome" is limited, suggesting that chaperoning effects have evolved to constrain self-complementary segments from interacting with each other [27]. Moreover, functional interactions may act as a survival strategy against abnormal aggregations [41].

3.2. Distinct expression pattern of human cathepsin F compared to its N-terminally truncated forms following overexpression in HEK 293T cells

Wild-type human cathepsin F (wtCatF) and its N-terminally truncated forms Ala^{20}–Asp^{484} (Δ^{19}CatF), Pro^{126}–Asp^{484} (Δ^{125}CatF) and Met^{147}–Asp^{484} (Δ^{146}CatF) were cloned into a pcDNA3 vector and used for transient transfection experiments on HEK 293T cells. Two constructs were generated by deletion of the first 19 amino acid residues (SP), which represent the enzyme's signal peptide (Δ^{19}CatF) and the cystatin-like domain [20] (Δ^{125}CatF), whereas the third construct (Δ^{146}CatF) also lacks a 20-amino acid residue-long linker region and represents the naturally truncated form of human cathepsin F, which was first obtained from a λgt10-skeletal muscle cDNA library [42]. A schematic representation of wtCatF and its N-terminally truncated forms (Δ^{19}CatF, Δ^{125}CatF and Δ^{146}CatF) is shown in Fig. 3.

Western blotting analysis of the soluble fraction highlights the successful expression of the wild-type protein, which was detected as a major band of ~70 kDa and a minor band of 30 kDa (Fig. 4A lane 4). As assessed from the protein sequence, the predicted Mw of human cathepsin F (Δ^{19}CatF) was 51.4 kDa, whereas the mature form of the enzyme exhibited a theoretical average Mw of 23.6 kDa. Thus, the higher values assessed by Western blotting analysis (Fig. 4A) could be attributed to the presence of five potential N-linked glycosylation sites, two of which are located in the enzyme's 251-amino acid long propeptide (Asn160, Asn195) and three sites are present in its mature form

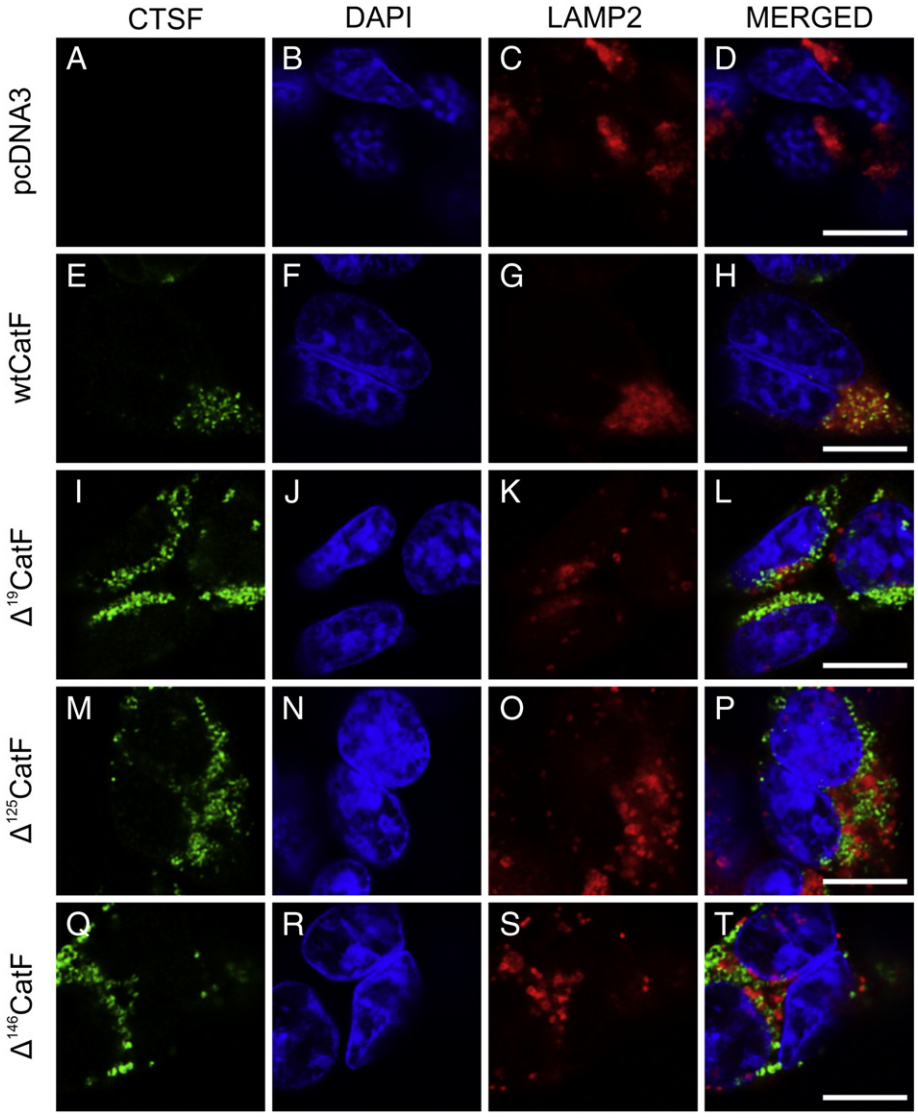

Fig. 6. Subcellular localization of human cathepsin F (E-H) and its N-terminally truncated forms Δ^{19}CatF (I–L), Δ^{125}CatF (M–P) and Δ^{146}CatF (Q–T). HEK 293T cells were transfected with wtCatF and its N-terminally truncated forms for 48 h. Their subcellular localizations were assessed using confocal microscopy and multiple immunofluorescence signals compared using anti-cathepsin F and anti-LAMP2 antibodies, followed by Alexa Fluor-labeled secondary antibodies as described in Section 2.9. Confocal images (optical sections) showed intracellular cathepsin F (CTSF) (green fluorescence: A, E, I, M, Q) together with the lysosomal marker LAMP2 (red fluorescence: C, G, K, O, S). Merged images showed overlapping immunoreactivity in yellow (D, H, L, P, T). The nucleus was counterstained for DNA using DAPI (blue fluorescence: B, F, J, N, R). Negative controls included the non-transfected, mock-transfected and pcDNA3 empty vector-transfected cells. Under these three conditions, a very similar pattern was obtained. Thus, as a representative example, only the pcDNA3 (A–D) example is shown. Scale bars = 10 μm.

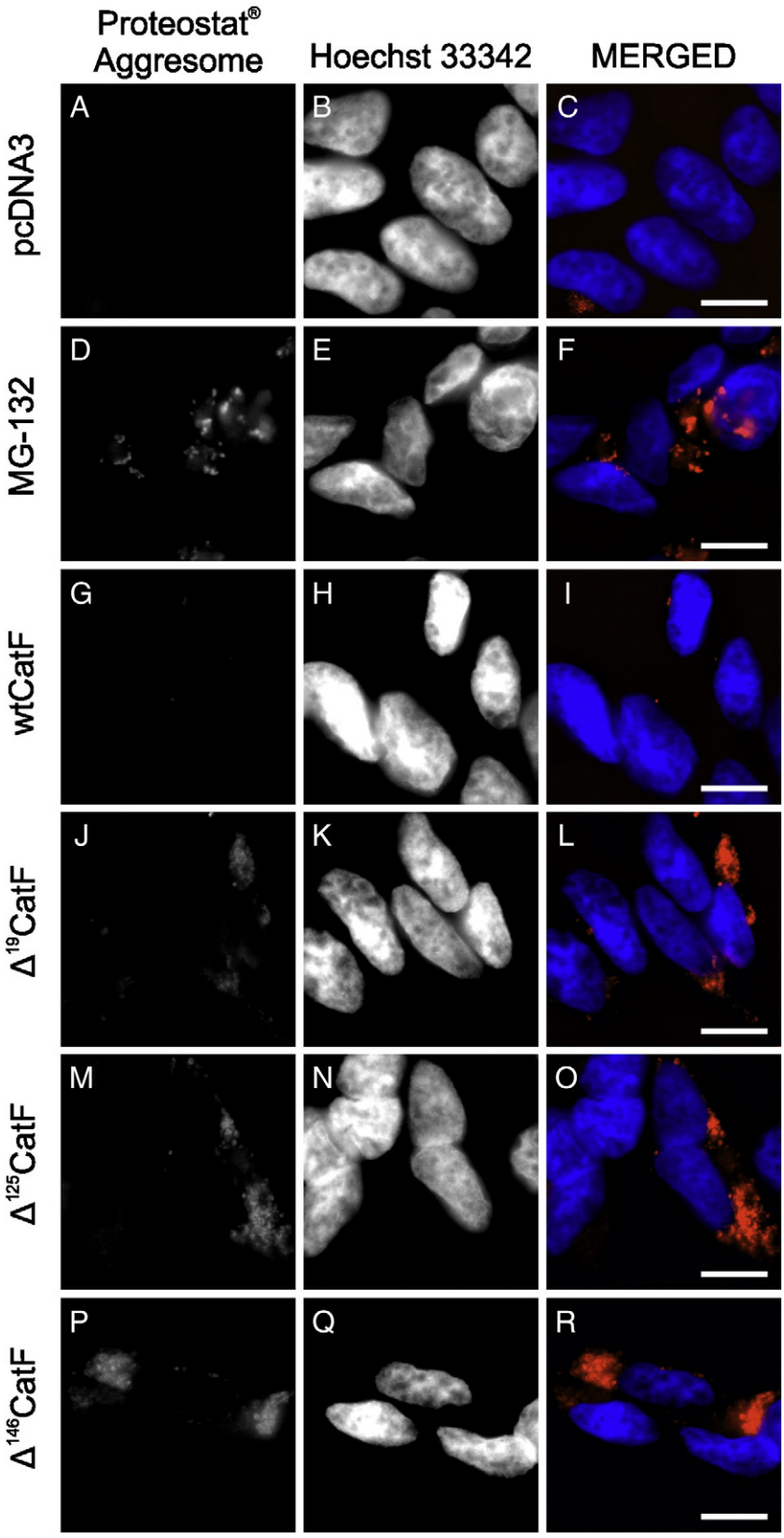

Fig. 7. Aggresome formation in HEK 293T cells 48 h post-transfection with pcDNA3-containing plasmids of human cathepsin F (G–I) and its N-terminally truncated forms Δ^{19}CatF (J–L), Δ^{125}CatF (M–O) and Δ^{146}CatF (P–R), as detected using the ProteoStat® aggresome detection dye. Δ^{19}CatF (J), Δ^{125}CatF (M) and Δ^{146}CatF (P) accumulated in aggresomes similar to cells pretreated with 5 μM of the proteasome inhibitor MG-132 (D). This was in contrast to the wild-type protein (wtCatF) (G) and empty vector-transfected negative control cells (A). The nucleus was counterstained for DNA using Hoechst 33342. Images were labeled with the ProteoStat® aggresome dye (A, D, G, J, M, P) and Hoechst 33342 nuclear stain (blue fluorescence: B, E, H, K, N, Q) and a merged view (C, F, I, L, O, R). The experiment was performed as previously described in Section 2.10. Negative controls included the non-transfected, mock-transfected and pcDNA3 empty vector-transfected cells. Under these three conditions, a very similar pattern was obtained. Thus, as a representative example, only the pcDNA3 (A–C) example is shown. Scale bars = 10 μm.

(Asn367, Asn378, Asn440) [20,42,43]. Using the peptide: N-glycosidase F (PNGase F), a potent enzyme with broader specificity that hydrolyzes all classes of asparagine-linked glycans [44], we demonstrated an approximate decrease of 6 kDa in the molecular mass of the full-length and mature forms of the enzyme, respectively (Fig. 4B). In vitro studies showed that treatment of the recombinant human cathepsin F zymogen with endoglycosidases H and F resulted in a decrease in the Mw of the proenzyme and mature form of approximately 9 kDa and 5 kDa, respectively [42,43]. Since PNGase F demonstrates an effect on most types of oligosaccharides, in particular, high mannose, hybrid, or complex type oligosaccharides [44], the observed differences were due to a different glycosylation pattern of recombinant human cathepsin F, which was produced in different expression systems [42,45]. Importantly, glycosylation pattern differences were found in proteins isolated from different tissues as well as transiently and permanently transfected cell lines [46,47].

Although all of the constructs were successfully transfected and the amount of protein loaded per lane was equivalent in all of the samples (20 μg), the N-terminally truncated forms of the enzyme, in particular, Δ^{19}CatF, Δ^{125}CatF and Δ^{146}CatF were nearly undetectable in the soluble fractions (Fig. 4A lanes 5–7). These results motivated the evaluation of the insoluble fraction. Interestingly, all of the evaluated N-terminally truncated forms of human cathepsin F were predominantly found in the insoluble fraction (Fig. 5 lanes 5–7), thus confirming that the deletion of at least the signal peptide (Fig. 5 lane 5), resulted in protein aggregation. Unexpectedly, Δ^{19}CatF was detected as a major band with a Mw of ~60 kDa, which was ~10 kDa smaller than its wild-type counterpart. In addition, two minor bands of 52 and 45 kDa, respectively, which were only observed in its truncated form (Fig. 5 lane 5). Moreover, Δ^{125}CatF and Δ^{146}CatF were detected as single bands with a Mw of 40 kDa (Fig. 5 lane 6) and 38 kDa (Fig. 5 lane 7), which were consistent with their theoretical average Mw of 39.9 kDa and 37.9 kDa, respectively.

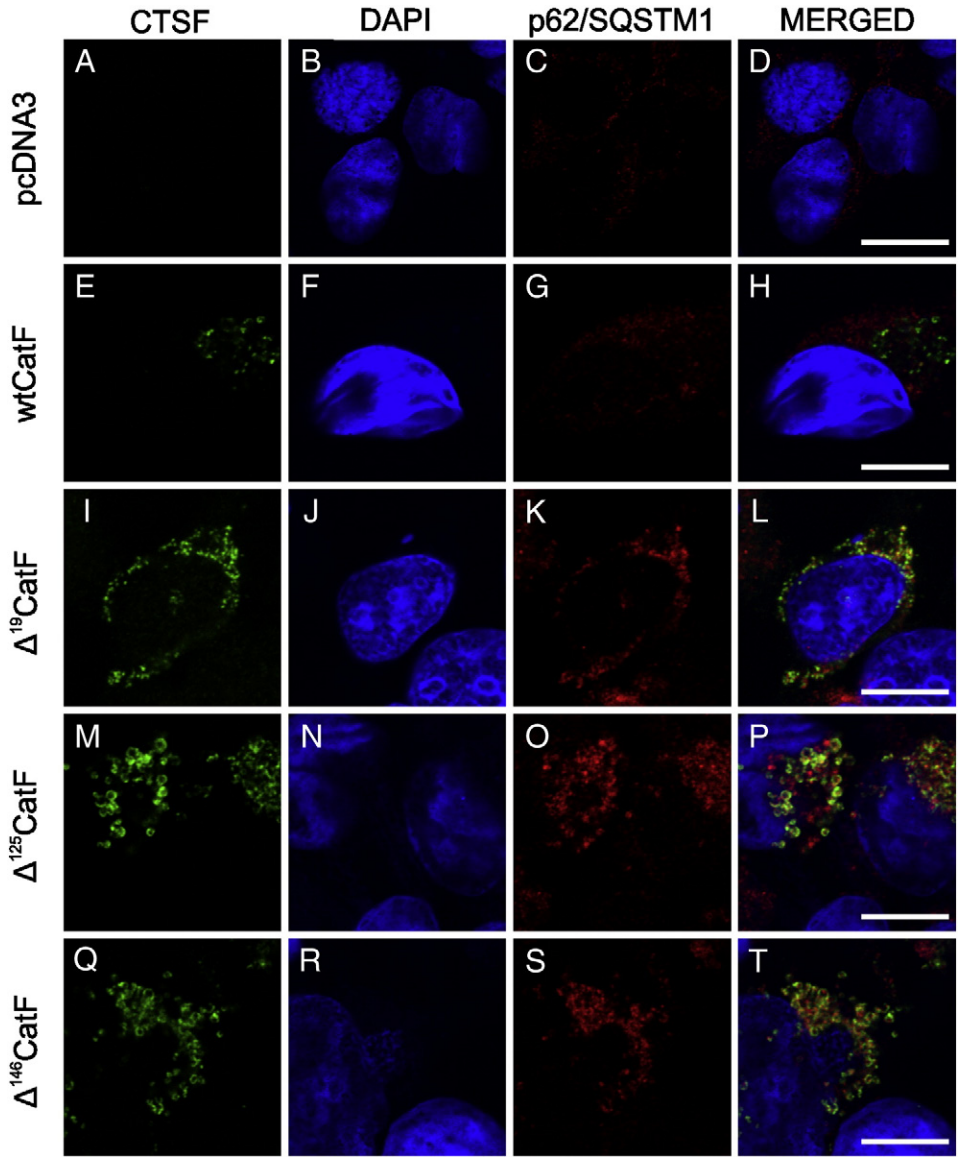

Fig. 8. N-terminally truncated forms of human cathepsin F Δ^{19}CatF (I–L), Δ^{125}CatF (M–P) and Δ^{146}CatF (Q–T) are p62-positive inclusions, which differ from the wild-type protein (E–H). HEK 293T cells were transfected with human cathepsin F and its N-terminally truncated forms for 48 h. Double immunolabeling with anti-cathepsin F and anti-p62/SQSTM1 antibodies, was performed as previously described in Section 2.9. Confocal images (optical sections) showed cathepsin F (CTSF) (green fluorescence: A, E, I, M, Q) and the p62/SQSTM1 marker (red fluorescence: C, G, K, O, S). Merged images showed overlapping immunoreactivity in yellow (D, H, L, P, T). The nucleus was counterstained for DNA using DAPI (blue fluorescence: B, F, J, N, R). Negative controls included the non-transfected, mock-transfected and pcDNA3 empty vector-transfected cells. Under these three conditions, a very similar pattern was obtained. Thus, as a representative example, only the pcDNA3 (A–D) example is shown. Scale bars = 10 μm.

3.3. N-terminally truncated forms of human cathepsin F in HEK 293T cells accumulated in aggresome-like inclusions and induce caspase activation, which differs from wild-type protein

Cysteine cathepsins require their propeptides for targeting and proper folding [48]. A strong correlation exists between the structural integrity of the propeptide, its inhibitory potency and its ability to catalyze the correct folding of the mature enzyme [48]. Similar to cathepsin L-like enzymes, human cathepsin F propeptide (Ser^{176}–Lys^{270}) [20] is present in Δ^{19}CatF and Δ^{125}CatF (as shown in this study) and the naturally occurring truncated form of the enzyme Met^{147}–Asp^{484} (Δ^{146}CatF) [42], suggesting that their folding properties are not compromised. Moreover, the latter has been confirmed to be catalytically active [42].

Transient transfections of wtCatF using HEK 293T cells showed a vesicular labeling pattern (Fig. 6E), which was characteristic of the lysosomal compartment (Fig. 6G) and was further confirmed by colocalization with LAMP2 (Fig. 6H). No fluorescence signal in green spectrum was detected with the empty vector-transfected cells (Fig. 6A, D). However, the N-terminally truncated forms Δ^{19}CatF, Δ^{125}CatF and Δ^{146}CatF were concentrated as large perinuclear–juxtanuclear aggregates (Fig. 6I, M, Q), which did not significantly colocalize with the lysosomal marker LAMP2 (Fig. 6L, P, T). Noteworthy, it was shown that the truncated forms of cathepsins B [18], H [49] and L [50], which contained a partial or total deletion of the signal peptide demonstrated altered trafficking and was thus targeted to the mitochondria, perinuclear, secreted, and nuclear sites, respectively.

The subcellular localization and labeling pattern observed for the N-terminally truncated forms of human cathepsin F motivated the hypothesis of whether the truncated forms reside within organelle-like structures, which are also known as aggresomes. Using a novel red fluorescent molecular rotor dye, which is essentially non-fluorescent until it binds to the structural features associated with aggregated protein

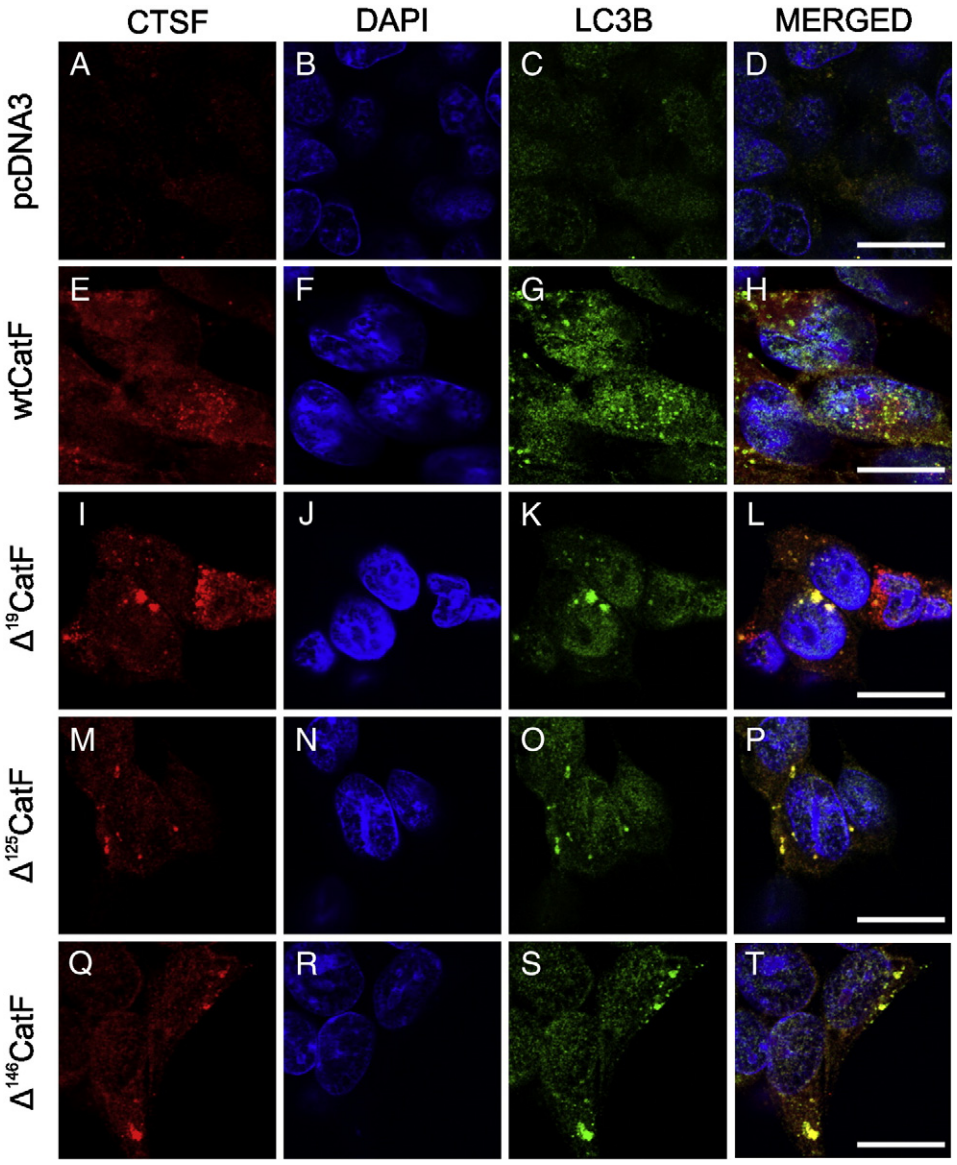

Fig. 9. Immunofluorescence of LC3B upon overexpression of human cathepsin F (E–H) and its N-terminally truncated forms Δ^{19}CatF (I–L), Δ^{125}CatF (M–P) and Δ^{146}CatF (Q–T). HEK 293T cells were transfected with human cathepsin F and its N-terminally truncated forms for 48 h. Double immunolabeling with anti-cathepsin F and anti-LC3B antibodies, was performed as described in Section 2.9. Confocal images (optical sections) showed human cathepsin F (CTSF) (red fluorescence: A, E, I, M, Q) and LC3B as marker of autophagy (green fluorescence: C, G, K, O, S). Merged images showed overlapping immunoreactivity in yellow (D, H, L, P, T). The nucleus was counterstained for DNA using DAPI (blue fluorescence: B, F, J, N, R). Negative controls included the non-transfected, mock-transfected and pcDNA3 empty vector-transfected cells. Under these three conditions, a very similar pattern was obtained. Thus, as a representative example, only the pcDNA3 (A–D) example is shown. Scale bars = 10 μm.

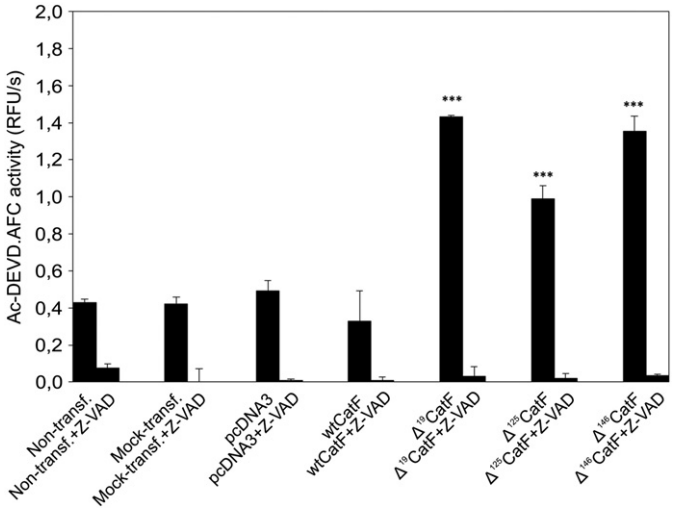

Fig. 10. Overexpression of the N-terminally truncated forms of human cathepsin F, but not the wild-type protein, induces caspase activation. DEVDase activity was monitored by kinetics 48 h post-transfection with pcDNA3-containing plasmids of human cathepsin F and its N-terminally truncated forms Δ^{19}CatF, Δ^{125}CatF and Δ^{146}CatF. Human cathepsin F (wtCatF) overexpression did not have an effect on caspase activation. In contrast, the N-terminally truncated forms Δ^{19}CatF, Δ^{125}CatF and Δ^{146}CatF induced an approximately 2–3 fold increase in DEVDase activity, which was blocked by the pan-caspase inhibitor Z-VAD(OMe)-FMK. Negative control experiments included non-transfected, mock-transfected and pcDNA3 empty vector-transfected cells. The results are given as the means ± SD of three independent experiments. ***, $p < 0.001$ compared to pcDNA3.

cargo [51], we demonstrated that the N-terminally truncated forms Δ^{19}CatF (Fig. 7J, L), Δ^{125}CatF (Fig. 7M, O) and Δ^{146}CatF (Fig. 7P, R) accumulated in aggresome-like inclusions. This was similar to observations made when autophagy was induced by treatment with the proteasome inhibitor MG-132 (Fig. 7D, F). In contrast, no effect was observed after the overexpression of wild-type protein (Fig. 7G, I) or empty vector-transfected cells (Fig. 7A, C). Next, we further examined whether the truncated forms of human cathepsin F might colocalize with an aggresome-related protein such as p62/SQSTM1. p62/SQSTM1 is a multifunctional polyubiquitin-binding protein that is commonly detected in cytoplasmic inclusions in diseases associated with protein aggregation [52]. In this study, all three human cathepsin F's N-terminally truncated forms (Fig. 8I, M, Q) had colocalized with p62/SQSTM1 (Fig. 8L, P, T), providing additional evidence that Δ^{19}CatF, Δ^{125}CatF and Δ^{146}CatF accumulated in aggresomes.

Aggresome formation was initially proposed as a general cellular response that occurred when the capacity of the proteasome was exceeded by the production of aggregation-prone misfolded proteins [23,53]. The aggregate-prone proteins would then be cleared from the cytosol by autophagy by removing the primary toxin (misfolded/aggregate-prone protein) and reducing its susceptibility to apoptotic insults [54]. However, recent evidence indicates that in mammalian cells, these aggresomes do not represent a general cellular response to protein misfolding [55,56].

To assess whether the protein aggregates induced by Δ^{19}CatF, Δ^{125}CatF and Δ^{146}CatF would be degraded and/or cleared via the autophagy pathway, we evaluated their potential colocalization with the autophagy marker, microtubule-associated protein 1A/1B-light chain 3 (LC3B) [57]. Interestingly, all three N-terminally truncated forms of cathepsin F (Fig. 9I, M, Q) were colocalized with LC3B (Fig. 9L, P, T), which indicated autophagy as a protective mechanism. In contrast, the wild-type protein exhibited a more diffuse vesicular pattern (Fig. 9H). Similarly, in huntingtin-induced cell death p62/SQSTM1 was shown to form protein aggregates that were degraded by autophagy [58]. Moreover, p62/SQSTM1 bound directly to Atg8/LC3 to facilitate the degradation of polyubiquitin-containing bodies by autophagy [59].

However, the accumulation of toxic proteins in the cytoplasm of neuronal and non-neuronal cells has also been linked to cytotoxicity and cell death by apoptosis [60–63]. Since Δ^{19}CatF, Δ^{125}CatF and Δ^{146}CatF accumulate in aggresome-like inclusions, we evaluated the potential contribution of apoptosis that was induced by caspase activation. An approximately 2–3 fold increase in DEVDase activity was evident in the samples transfected with the N-terminally truncated forms of the enzyme and was blocked by the general caspase inhibitor Z-VAD(OMe)-FMK (Fig. 10).

Transient overexpression of wtCatF did not induce caspase activation (Fig. 10), which is consistent with reports on cathepsins B and L [15]. Moreover, annexin V/propidium iodide staining and flow cytometry analysis 48 h post-transfection revealed that the number of apoptotic cells was below 5–10% after overexpression of wtCatF and its N-terminally truncated forms compared to non-transfected, mock-transfected and pcDNA3 empty vector-transfected cells (results not shown). Thus, the resulting DEVDase activity in our cellular model was not sufficient to induce apoptotic cell death. However, cathepsin B alternatively spliced variants [16,18] and its artificially truncated forms [17] resulted in nuclear fragmentation and cell death. Alternatively spliced variants and/or truncated forms of different cathepsins where found in different subcellular compartments i.e. aggresomes (this study), cytoplasm, mitochondria, nuclear, perinuclear and secreted [16–18,49,50]. Their effects on the cell were either deleterious, similar to reports for cathepsin B transcripts lacking exons 2 and 3 with and without the C-terminal propeptide and other aberrant forms [16–18] or did not manifest signs of cell death such as in cathepsin B transcripts with or without exon 2, in the presence of the C-terminal propeptide [16]. The N-terminally truncated forms of cathepsin F (in this study), showed many potential future avenues to pursue to gain insight into the role of cathepsins in pathophysiology. A genome-wide linkage mapping study of two families with recessive type B Kufs disease, an adult-onset neuronal ceroid lipofuscinosis, detected five rare or novel pathogenic mutations within human cathepsin F (CTSF). The authors proposed that CTSF should receive the locus designation CLN13 [64]. Moreover, the single nucleotide frameshift deletion in exon 7 (c.954delC [pSer319Leufs*27]) resulted in a nonsense mutation that truncated the protein to approximately three-quarters of its normal length [64].

4. Conclusion

In summary, we predicted that human cathepsin F contained three natively disordered regions within the enzyme's propeptide and various aggregation-prone amino acid stretches. Our results confirmed that the N-terminally truncated forms of human cathepsin F were found concentrated as large perinuclear-juxtanuclear aggregates, which accumulated within aggresome-like inclusions, and are cleared via the p62/SQSTM1-dependent autophagy pathway. In addition, an approximately 2–3 fold increase in DEVDase activity was not sufficient to induce apoptotic cell death. Furthermore, the truncated forms of cathepsins represent a wide signaling repertoire that is worth pursuing in future studies in order to gain insight into their role in pathophysiology.

Acknowledgements

The authors are grateful to Prof. Guy Salvesen (Sanford-Burnham Institute for Medical Research, La Jolla, CA, USA) and Dr. Urška Repnik for their valuable discussions. Confocal microscopy has been performed within Leica Reference Centre for confocal microscopy with white light laser (WLL) in Ljubljana. This study was supported by grants J1-9520 and J3-2258 to V.S., and P1-0140 to B.T obtained from the Slovenian Research Agency—ARRS.

References

[1] V. Turk, V. Stoka, O. Vasiljeva, M. Renko, T. Sun, B. Turk, D. Turk, Cysteine cathepsins: from structure, function and regulation to new frontiers, Biochim. Biophys. Acta 1824 (2012) 68–88.
[2] B. Turk, V. Stoka, J. Rozman-Pungerčar, T. Cirman, G. Droga-Mazovec, K. Orešić, V. Turk, Apoptotic pathways: involvement of lysosomal proteases, Biol. Chem. 383 (2002) 1035–1044.
[3] M.E. Guicciardi, M. Leist, G.J. Gores, Lysosomes in cell death, Oncogene 23 (2004) 2881–2890.
[4] P. Boya, G. Kroemer, Lysosomal membrane permeabilization in cell death, Oncogene 27 (2008) 6434–6451.
[5] T. Kirkegaard, M. Jäättelä, Lysosomal involvement in cell death and cancer, Biochim. Biophys. Acta 1793 (2009) 746–754.
[6] U. Repnik, V. Stoka, V. Turk, B. Turk, Lysosomes and lysosomal cathepsins in cell death, Biochim. Biophys. Acta 1824 (2012) 22–33.
[7] C. Tardy, P. Codogno, H. Autefage, T. Levade, N. Andrieu-Abadie, Lysosomes and lysosomal proteins in cancer cell death (new players of an old struggle), Biochim. Biophys. Acta 1765 (2006) 101–125.
[8] M.E. Guicciardi, J. Deussing, H. Miyoshi, S.F. Bronk, P.A. Svingen, C. Peters, S.H. Kaufmann, G.J. Gores, Cathepsin B contributes to TNF-α-mediated hepatocyte apoptosis by promoting mitochondrial release of cytochrome c, J. Clin. Invest. 106 (2000) 1127–1137.
[9] V. Stoka, B. Turk, S.L. Schendel, T.H. Kim, T. Cirman, S.J. Snipas, L.M. Ellerby, D. Bredesen, H. Freeze, M. Abrahamson, D. Brömme, S. Krajewski, J.C. Reed, X.M. Yin, V. Turk, G.S. Salvesen, Lysosomal protease pathways to apoptosis: cleavage of Bid, not pro-caspases, is the most likely route, J. Biol. Chem. 276 (2001) 3149–3157.
[10] L. Bojič, A. Petelin, V. Stoka, T. Reinheckel, C. Peters, V. Turk, B. Turk, Cysteine cathepsins are not involved in Fas/CD95 signalling in primary skin fibroblasts, FEBS Lett. 581 (2007) 5185–5190.
[11] P. Boya, K. Andreau, D. Poncet, N. Zamzami, J.L. Perfettini, D. Metivier, D.M. Ojcius, M. Jäättelä, G. Kroemer, Lysosomal membrane permeabilization induces cell death in a mitochondrion-dependent fashion, J. Exp. Med. 197 (2003) 1323–1334.
[12] G. Droga-Mazovec, L. Bojič, A. Petelin, S. Ivanova, R. Romih, U. Repnik, G.S. Salvesen, V. Stoka, V. Turk, B. Turk, Cysteine cathepsins trigger caspase-dependent cell death through cleavage of bid and antiapoptotic Bcl-2 homologues, J. Biol. Chem. 283 (2008) 19140–19150.
[13] M. Klarić, S. Tao, V. Stoka, B. Turk, V. Turk, Cysteine cathepsins are not critical for TNF-α-induced cell death in T98G and U937 cells, Biochim. Biophys. Acta 1794 (2009) 1372–1377.
[14] L.P. Deiss, H. Galinka, H. Berissi, O. Cohen, A. Kimchi, Cathepsin D protease mediates programmed cell death induced by interferon-γ, Fas/APO-1 and TNF-α, EMBO J. 15 (1996) 3861–3870.
[15] A. Gewies, S. Grimm, Cathepsin-B and cathepsin-L expression levels do not correlate with sensitivity of tumour cells to TNF-α-mediated apoptosis, Br. J. Cancer 89 (2003) 1574–1580.
[16] K. Müntener, R. Zwicky, G. Csucs, A. Baici, The alternative use of exons 2 and 3 in cathepsin B mRNA controls enzyme trafficking and triggers nuclear fragmentation in human cells, Histochem. Cell Biol. 119 (2003) 93–101.
[17] F. Bestvater, C. Dallner, E. Spiess, The C-terminal subunit of artificially truncated human cathepsin B mediates its nuclear targeting and contributes to cell viability, BMC Cell Biol. 6 (2005) 16.
[18] K. Müntener, R. Zwicky, G. Csucs, J. Rohrer, A. Baici, Exon skipping of cathepsin B: Mitochondrial targeting of a lysosomal peptidase provokes cell death, J. Biol. Chem. 279 (2004) 41012–41017.
[19] C.M. Haraguchi, T. Mabuchi, S. Hirata, T. Shoda, K. Hoshi, K. Akasaki, S. Yokota, Chromatoid bodies: aggresome-like characteristics and degradation sites for organelles of spermiogenic cells, J. Histochem. Cytochem. 53 (2005) 455–465.
[20] D.K. Nägler, T. Sulea, R. Ménard, Full-length cDNA of human cathepsin F predicts the presence of a cystatin domain at the N-terminus of the cysteine protease zymogen, Biochem. Biophys. Res. Commun. 257 (1999) 313–318.
[21] I. Santamaría, G. Velasco, A.M. Pendás, A. Paz, C. López-Otín, Molecular cloning and structural and functional characterization of human cathepsin F, a new cysteine proteinase of the papain family with a long propeptide domain, J. Biol. Chem. 274 (1999) 13800–13809.
[22] C.H. Tang, J.W. Lee, M.G. Galvez, L. Robillard, S.E. Mole, H.A. Chapman, Murine cathepsin F deficiency causes neuronal lipofuscinosis and late-onset neurological disease, Mol. Cell. Biol. 26 (2006) 2309–2316.
[23] J.A. Johnston, C.L. Ward, R.R. Kopito, Aggresomes: a cellular response to misfolded proteins, J. Cell Biol. 143 (1998) 1883–1898.
[24] E. Gasteiger, C. Hoogland, A. Gattiker, S. Duvaud, M.R. Wilkins, R.D. Appel, A. Bairoch, Protein identification and analysis tools on the ExPASy server, in: J.M. Walker (Ed.), The proteomics protocols handbook, Humana Press, 2005, pp. 571–607.
[25] T. Ishida, K. Kinoshita, Prediction of disordered regions in proteins based on the meta approach, Bioinformatics 24 (2008) 1344–1348.
[26] M.J. Thompson, S.A. Sievers, J. Karanicolas, M.I. Ivanova, D. Baker, D. Eisenberg, The 3D profile method for identifying fibril-forming segments of proteins, Proc. Natl. Acad. Sci. U. S. A. 103 (2006) 4074–4078.
[27] L. Goldschmidt, P.K. Teng, R. Riek, D. Eisenberg, Identifying the amylome, proteins capable of forming amyloid-like fibrils, Proc. Natl. Acad. Sci. U. S. A. 107 (2010) 3487–3492.
[28] Y. Zhang, I-TASSER server for protein 3D structure prediction, BMC Bioinformatics 9 (2008) 40.
[29] A. Roy, A. Kucukural, Y. Zhang, I-TASSER: a unified platform for automated protein structure and function prediction, Nat. Protoc. 5 (2010) 725–738.
[30] S. Ventura, Sequence determinants of protein aggregation: tools to increase protein solubility, Microb. Cell Fact. 4 (2005) 11.
[31] C. Wurth, W. Kim, M.H. Hecht, Combinatorial approaches to probe the sequence determinants of protein aggregation and amyloidogenicity, Protein Pept. Lett. 13 (2006) 279–286.
[32] A.K. Dunker, J.D. Lawson, C.J. Brown, R.M. Williams, P. Romero, J.S. Oh, C.J. Oldfield, A.M. Campen, C.M. Ratliff, K.W. Hipps, J. Ausio, M.S. Nissen, R. Reeves, C. Kang, C.R. Kissinger, R.W. Bailey, M.D. Griswold, W. Chiu, E.C. Garner, Z. Obradovic, Intrinsically disordered protein, J. Mol. Graph. Model. 19 (2001) 26–59.
[33] R. Linding, J. Schymkowitz, F. Rousseau, F. Diella, L. Serrano, A comparative study of the relationship between protein structure and beta-aggregation in globular and intrinsically disordered proteins, J. Mol. Biol. 342 (2004) 345–353.
[34] M. Belli, M. Ramazzotti, F. Chiti, Prediction of amyloid aggregation in vivo, EMBO Rep. 12 (2011) 657–663.
[35] S.J. Hamodrakas, Protein aggregation and amyloid fibril formation prediction software from primary sequence: towards controlling the formation of bacterial inclusion bodies, FEBS J. 278 (2011) 2428–2435.
[36] M.R. Sawaya, S. Sambashivan, R. Nelson, M.I. Ivanova, S.A. Sievers, M.I. Apostol, M.J. Thompson, M. Balbirnie, J.J.W. Wiltzius, H.T. McFarlane, A.Ø. Madsen, C. Riekel, D. Eisenberg, Atomic structures of amyloid cross-β spines reveal varied steric zippers, Nature 447 (2007) 453–457.
[37] F. Chiti, C.M. Dobson, Protein misfolding, functional amyloid, and human disease, Annu. Rev. Biochem. 75 (2006) 333–366.
[38] R. Nelson, D. Eisenberg, Recent atomic models of amyloid fibril structure, Curr. Opin. Struct. Biol. 16 (2006) 260–265.
[39] R.S. Harrison, P.C. Sharpe, Y. Singh, D.P. Fairlie, Amyloid peptides and proteins in review, Rev. Physiol. Biochem. Pharmacol. 159 (2007) 1–77.
[40] J. Reumers, F. Rousseau, J. Schymkowitz, Multiple evolutionary mechanisms reduce protein aggregation, Open Biol. 2 (2009) 176–184.
[41] L. Masino, G. Nicastro, L. Calder, M. Vendruscolo, A. Pastore, Functional interactions as a survival strategy against abnormal aggregation, FASEB J. 25 (2011) 45–54.
[42] B. Wang, G.P. Shi, P.M. Yao, Z. Li, H.A. Chapman, D. Brömme, Human cathepsin F. Molecular cloning, functional expression, tissue localization, and enzymatic characterization, J. Biol. Chem. 273 (1998) 32000–32008.
[43] J.D. Ho, Y. Meltser, J.J. Buggy, J.T. Palmer, K.C. Elrod, H. Chan, K.D. Mortara, J.R. Somoza, Expression, purification, crystallization and preliminary X-ray diffraction studies of human cathepsin F complexed with an irreversible vinyl sulfone inhibitor, Acta Crystallogr. D 58 (2002) 2187–2190.
[44] A.L. Tarentino, C.M. Gomez, T.H. Plummer, Deglycosylation of asparagine-linked glycans by peptide: N-glycosidase F, Biochemistry 24 (1985) 4665–4671.
[45] M. Fonovič, D. Brömme, V. Turk, B. Turk, Human cathepsin F: expression in baculovirus system, characterization and inhibition by protein inhibitors, Biol. Chem. 385 (2004) 505–509.
[46] C. Ohl, C. Albach, P. Altevogt, B. Schmitz, N-glycosylation patterns of HSA/CD24 from different cell lines and brain homogenates: a comparison, Biochimie 85 (2003) 565–573.
[47] . A.C. Vestrheim, A. Moen, W. Egge-Jacobsen, D.B. Bratlie, T.E. Michaelsen, Different glycosylation pattern of human IgG1 and IgG3 antibodies isolated from transiently as well as permanently transfected cell lines, Scand. J. Immunol. 77 (2013) 419–428.
[48] B. Wiederanders, Structure-function relationships in class CA1 cysteine peptidase propeptides, Acta Biochim. Pol. 50 (2003) 691–713.
[49] A. Waghray, D. Keppler, B.F. Sloane, L. Schuger, Y.Q. Chen, Analysis of a truncated form of cathepsin H in human prostate tumor cells, J. Biol. Chem. 277 (2002) 11533–11538.
[50] B. Goulet, A. Baruch, N.-S. Moon, M. Poirier, L.L. Sansregret, A. Erickson, M. Bogyo, A. Nepveu, A cathepsin L isoform that is devoid of a signal peptide localizes to the nucleus in S phase and processes the CDP/Cux transcription factor, Mol. Cell 14 (2004) 207–219.
[51] D. Shen, J. Coleman, E. Chan, T.P. Nicholson, L. Dai, P.W. Sheppard, W.F. Patton, Novel cell- and tissue-based assays for detecting misfolded and aggregated protein accumulation within aggresomes and inclusion bodies, Cell Biochem. Biophys. 60 (2011) 173–185.
[52] K. Zatloukal, C. Stumptner, A. Fuchsbichler, H. Heid, M. Schnoelzer, L. Kenner, R. Kleinert, M. Prinz, A. Aguzzi, H. Denk, p62 Is a common component of cytoplasmic inclusions in protein aggregation diseases, Am. J. Pathol. 160 (2002) 255–263.
[53] R. García-Mata, Z. Bebök, E.J. Sorscher, E.S. Sztul, Characterization and dynamics of aggresome formation by a cytosolic GFP-chimera, J. Cell Biol. 146 (1999) 1239–1254.
[54] A. Williams, L. Jahreiss, S. Sarkar, S. Saiki, F.M. Menzies, B. Ravikumar, D.C. Rubinsztein, Aggregate-prone proteins are cleared from the cytosol by autophagy: therapeutic implications, Curr. Top. Dev. Biol. 76 (2006) 89–101.
[55] S. Beaudoin, K. Goggin, C. Bissonnette, C. Grenier, X. Roucou, Aggresomes do not represent a general cellular response to protein misfolding in mammalian cells, BMC Cell Biol. 9 (2008) 59.
[56] E.S.P. Wong, J.M.M. Tan, W.E. Soong, K. Hussein, N. Nukina, V.I. Dawson, T.M. Dawson, A.M. Cuervo, K.L. Lim, Autophagy-mediated clearance of aggresomes is not a universal phenomenon, Hum. Mol. Genet. 17 (2008) 2570–2582.
[57] I. Tanida, T. Ueno, E. Kominami, LC3 and autophagy, Methods Mol. Biol. 445 (2008) 77–88.
[58] G. Bjørkøy, T. Lamark, A. Brech, H. Outzen, M. Perander, A. Øvervatn, H. Stenmark, T. Johansen, p62/SQSTM1 forms protein aggregates degraded by autophagy and has a protective effect on huntingtin-induced cell death, J. Cell Biol. 171 (2005) 603–614.
[59] S. Pankiv, T.H. Clausen, T. Lamark, A. Brech, J.-A. Bruun, H. Outzen, A. Øvervatn, G. Bjørkøy, T. Johansen, p62/SQSTM1 binds directly to Atg8/LC3 to facilitate degradation of ubiquitinated protein aggregates by autophagy, J. Biol. Chem. 282 (2007) 24131–24145.
[60] C. Grenier, C. Bissonnette, L. Volkov, X. Roucou, Molecular morphology and toxicity of cytoplasmic prion protein aggregates in neuronal and non-neuronal cells, J. Neurochem. 97 (2006) 1456–1466.

[61] M. Kristiansen, M.J. Messenger, P.C. Klöhn, S. Brandner, J.D.F. Wadsworth, J. Collinge, S.J. Tabrizi, Disease-related prion protein forms aggresomes in neuronal cells leading to caspase activation and apoptosis, J. Biol. Chem. 280 (2005) 38851–38861.
[62] X.L. Li, G.R. Wang, Y.Y. Jing, M.M. Pan, C.F. Dong, R.M. Zhou, Z.Y. Wang, Q. Shi, C. Gao, X.P. Dong, Cytosolic PrP induces apoptosis of cell by disrupting microtubule assembly, J. Mol. Neurosci. 43 (2011) 316–325.
[63] X. Wang, C.F. Dong, Q. Shi, S. Shi, G.R. Wang, Y.J. Lei, K. Xu, R. An, J.M. Chen, H.Y. Jiang, C. Tian, C. Gao, Y.J. Zhao, J. Han, X.P. Dong, Cytosolic prion protein induces apoptosis in human neuronal cell SH-SY5Y via mitochondrial disruption pathway, BMB Rep. 42 (2009) 444–449.
[64] K.R. Smith, H.-H.M. Dahl, L. Canafoglia, E. Andermann, J. Damiano, M. Morbin, A.C. Bruni, G. Giaccone, P. Cossette, P. Saftig, J. Grötzinger, M. Schwake, F. Andermann, J.F. Staropoli, K.B. Sims, S.E. Mole, S. Franceschetti, N.A. Alexander, J.D. Cooper, H.A. Chapman, S. Carpenter, S.F. Berkovic, M. Bahlo, Cathepsin F mutations cause type B Kufs disease, an adult-onset neuronal ceroid lipofuscinosis, Hum. Mol. Genet. 22 (2013) 1417–1423.
[65] W.L. DeLano, The PyMOL molecular graphics system, Computer Program, 2002, DeLano Scientific, San Carlos, CA, USA, 2002.